Heavy Metal Removal and Recovery by Contained Liquid Membrane Permeator

Asim K. Guha, Chang H. Yun, Rahul Basu, and Kamalesh K. Sirkar
Dept. of Chemistry and Chemical Engineering, Stevens Institute of Technology, Hoboken, NJ 07030

Heavy metals like Cu^{2+}, Cr^{6+}, and Hg^{2+} were removed successfully from wastewater and concentrated in a strip aqueous solution for recycle using the hollow-fiber-contained liquid membrane (HFCLM) technique. Using cotransport, Cr^{6+} and Hg^{2+} present as anions in the feed solution were transferred individually through a liquid membrane containing tri-n-octylamine in xylene and concentrated in an alkaline solution on the strip side. The removal efficiency of each heavy metal was studied as a function of the aqueous feed flow rate in an HFCLM permeator. Copper present as cation Cu^{2+} was removed and concentrated by countertransport using LIX84 in n-heptane as the liquid membrane. The efficiency of copper removal was studied as a function of feed copper concentration, feed flow rate, strip flow rate, and area ratio between the feed fiber set and strip fiber set. The strip side flow rate did not affect the Cu^{2+} transfer rate. A theoretical model presented predicts the copper transport rate from the feed solution to the strip solution in an HFCLM permeator with a variable feed to strip-side membrane area. Both feed aqueous boundary layer and interfacial complexation reaction on the feed side dominate the observed Cu^{2+} removal process through LIX 84 in n-heptane for feed concentration levels used 90-500 mg/L. It was verified by providing two times larger liquid-liquid interfacial area in the feed aqueous side or in the strip aqueous side. The model can be used to design the membrane area required on the feed and strip fiber sides to remove essentially all of the copper from a given wastewater stream.

Introduction

Efficient removal and recovery of toxic heavy metals from industrial waste streams prior to discharge is a major challenge. Not only does it eliminate toxicity but also it prevents metal accumulation in biological sludge. Although precipitation, ion exchange, or reverse osmosis (Williams et al., 1992) can remove heavy metals from water, they create an additional sludge and/or are costly.

An alternative is metal removal by a water insoluble metal-complexing extracting agent in a nonpolar organic solvent/diluent followed by stripping and concentration of the metal from the organic phase into an aqueous strip solution for metal recycle to the industrial process. Capital and energy costs of handling large solvent volumes and solvent loss by emulsion formation in such extractions have prompted the use of liquid membranes where extracting solvent inventory is reduced by orders of magnitude. A common liquid membrane configuration is the supported liquid membrane (SLM): the organic liquid membrane is present in the pores of a polymeric support membrane where the metal is extracted into the pore liquid at the feed solution-membrane interface. At the strip solution-membrane interface, the metal is back extracted and concentrated in the strip solution for recycle. Yi and Tavlarides (1992) have studied the kinetics of extraction and stripping of Cu^{2+} using the SLM configuration of the liquid ion exchanger in a porous ceramic support.

However, SLMs suffer from instability resulting from loss of membrane by solubility, osmotic flow of water across the membrane, progressive wetting of the support pores, and the

Correspondence concerning this article should be addressed to K. K. Sirkar.
Current address of A. K. Guha and K. K. Sirkar: Dept. of Chemical Engineering, Chemistry and Environmental Science, New Jersey Institute of Technology, Newark, NJ 07102.
Current address of C. H. Yun: Korea Explosives Group, Daejon, Korea.
Current address of R. Basu: Dept. of Chemical Engineering, University of Arkansas, Fayetteville, AR 72701.

pressure differential across the membrane (Danesi, 1984, 1985; Danesi et al., 1987). The other technique of emulsion liquid membrane (ELM) suffers from swelling instability of inner phase (Thien et al., 1986); further, it requires emulsification and demulsification, the latter step being especially problematic.

A novel but robust liquid membrane technique has been recently developed (Sengupta et al., 1988a,b; Basu and Sirkar, 1991, 1992; Sorenson and Callahan, 1990). Here the extracting organic solvent is contained in the interstices of two well packed sets of microporous hollow fibers (MHF) in the shellside of a MHF permeator. In this hollow-fiber-contained liquid membrane (HFCLM) technique, the dilute aqueous feed flows in the lumen of one set of fibers. The aqueous strip solution passes through the lumen of the other fiber set. Each aqueous-organic phase interface is immobilized at the pore-mouths of the respective fiber since the correct range of phase pressure conditions (Kiani et al., 1984; Prasad and Sirkar, 1987, 1988) are easily maintained (Sengupta et al., 1988a,b). For hydrophobic fibers, the aqueous feed and strip solutions flow at pressures higher than the organic liquid membrane pressure set independently by the membrane liquid reservoir which automatically replaces any membrane liquid lost to the feed and strip solutions.

Heavy metals are generally present in wastewater either as a cation or as an anion. Cations are usually extracted into an organic diluent by acidic or chelating extractants and anionic species containing metal in an aqueous solution can be extracted via ion-pair formation with long chain alkyl amines in an organic diluent in the presence of salts or acids in the aqueous phase (Ritcey and Ashbrook, 1984).

Copper has been selectively recovered from a feed aqueous solution and concentrated in a highly acidic solution by coupled-transport in a pH gradient across a liquid membrane containing a liquid ion exchanger LIX 64N (Lee et al., 1978; Pearson, 1983) according to the following reaction:

$$2\overline{RH} + Cu^{2+} \rightleftharpoons \overline{R_2Cu} + 2H^+ \qquad (1)$$

where RH stands for the liquid ion exchanger. Overbar indicates the organic medium. Transport of Cu^{2+} via the coupled-transport mechanism is shown in Figure 1. For Cu^{2+} removal and recovery, Kim (1984) had also used LIX 64N in two hollow fiber membrane extractors, one for extraction where forward reaction 1 takes place and the other one for stripping where extractant is regenerated by the backward reaction 1. Thus, in the liquid membrane device, be it an SLM or an HFCLM, the two different extractors are combined in one device with no movement of the organic liquid extractant. However, contrary to SLM, HFCLM can be operated with a moving liquid membrane.

Cr^{6+} from wastewater has been removed by cotransport through an organic liquid membrane using tertiary amine (R_3N) as a carrier which forms a complex with proton and a hydrogen chromate (Hochhauser and Cussler, 1975) according to the following forward reaction:

$$HCrO_4^-(aq) + H^+(aq) + 2R_3N(org) \rightarrow (R_3NH)_2CrO_4(org) \qquad (2)$$

It is then concentrated in the alkaline strip solution via:

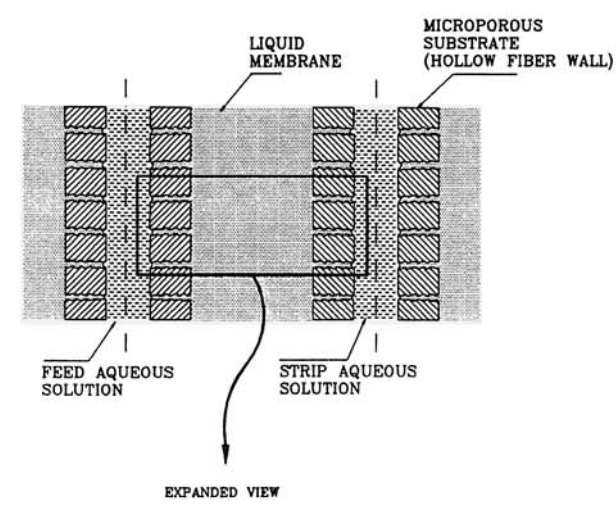

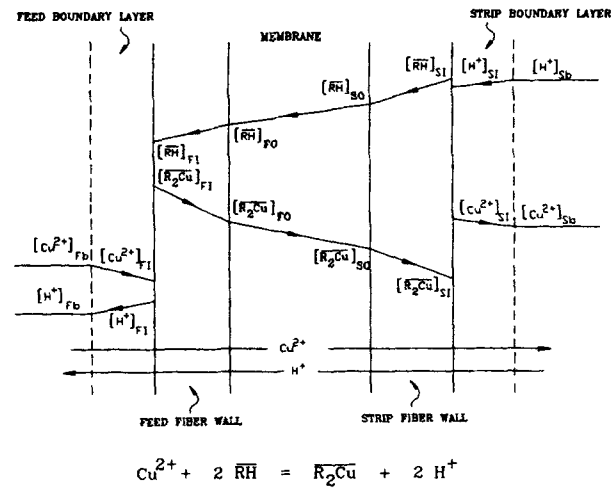

$$Cu^{2+} + 2\,\overline{RH} = \overline{R_2Cu} + 2\,H^+$$

Figure 1. Concentration profiles of Cu^{2+} and H^+ across the liquid membrane.

$$(R_3NH)_2CrO_4(org) + 2OH^-(aq) \rightarrow 2R_3N(org) + CrO_4^{2-}(aq) + 2H_2O(aq) \qquad (3)$$

Chromium recovery from electroplating baths using a similar liquid membrane has also been demonstrated but a rapid flux decline was observed (Pearson, 1983). Teramoto et al. (1989) studied the performance of removal of Cr^{6+} from an aqueous solution by reaction 2 and recovery into an aqueous solution according to reaction 3 via a moving liquid membrane in a spiral-wound module using tri-*n*-octylamine as the carrier.

Mercuric chloride has been extracted efficiently from a solution of low pH ($\sim$2-3) by a tertiary amine in xylene according to reaction 4 given below and then separately stripped successfully into an alkaline solution of pH 9-10 (Caban and Chapman, 1972). Extraction and stripping proceeds respectively according to:

$$HgCl_2(aq) + 2HCl(aq) + 2R_3N(org) \rightarrow (R_3NH)_2HgCl_4(org) \qquad (4)$$

$$(R_3NH)_2HgCl_4(org) + 2OH^-(aq) \rightarrow 2R_3N(org) + 2Cl^-(aq) + HgCl_2(aq) + 2H_2O(aq) \qquad (5)$$

Transport of Hg^{2+} through a liquid membrane (tertiary amine in a diluent) also follows the cotransport mechanism. Hg^{2+} from wastewater has been removed and concentrated by a countertransport mechanism similar to that for copper ion using an emulsion liquid membrane (Weiss et al., 1982).

HFCLM technique can offer a practical alternative to current techniques and processes for removal of heavy metals from aqueous stream and concentrating them into a strip aqueous stream. This can be achieved either by a cotransport or countertransport mechanism depending on the ions being transferred and the type of carrier being used. We present here a comprehensive investigation of simultaneous removal of Cu^{2+} from wastewaters and its concentration in an aqueous strip solution by an HFCLM permeator. The objective is to analyze the behavior of the permeator as the wastewater feed containing 100–500 mg/L of Cu^{2+} as cupric sulfate is purified to low levels while the strip solution gets concentrated to high levels of Cu^{2+}. The carrier used for Cu^{2+} is LIX 84 in *n*-heptane. We have systematically studied the effects of flow rate variations, variations of the LIX 84 concentration in the diluent, *n*-heptane, and the variations of the interfacial areas between the feed-solution-membrane interface and the strip-solution-membrane interface. This last aspect is especially novel and is possible only in an HFCLM permeator. It allows, for example, maximization of feed-solution-membrane interfacial area if the feed interfacial reaction provides the controlling resistance.

We have also developed a permeator model that incorporates various steps in the transport of Cu^{2+} from the feed solution to the strip solution and compared its predictions with the experimental results. This study of HFCLM permeator-based Cu^{2+} removal from wastewater is in contrast to the nondispersive, microporous membrane-based solvent extraction in a membrane-module having only one set of fibers (Yun et al., 1993); the latter will require a separate module where back extraction into the aqueous strip has to be carried out with the extractant being mobile.

We have also investigated experimentally the individual removal of Cr^{6+} and Hg^{2+} from simulated wastewaters and their simultaneous concentration in a strip aqueous stream by means of an HFCLM permeator. The carrier used in both cases was tri-*n*-octylamine in xylene. We illustrate here the capabilities of HFCLM permeator in reducing the concentration of these toxic metals from 100–250 mg/L to very low levels as these metals are simultaneously concentrated to a high concentration level in the strip solution.

Experimental Details

Distribution coefficients and analytical protocols

Organic extractants selected were 10–20% v/v LIX 84 (Henkel, Tucson, AZ) diluted in *n*-heptane (Aldrich, Milwaukee, WI) for Cu^{2+} and 20% v/v tri-*n*-octylamine (TOA) (Fluka, Ronkonkoma, NY) diluted in xylene (Fisher, Springfield, NJ) for Cr^{6+} and Hg^{2+}. 5% v/v 2-ethyl-1-hexanol (Aldrich, Milwaukee, WI) was added to the organic extractant as a modifier to prevent the formation of an organic precipitate during chromium extraction with TOA. Copper sulfate pentahydrate (Fluka, Ronkonkoma, NY), potassium dichromate and mercury (II) chloride (Aldrich, Milwaukee, WI) were separately dissolved in deionized water to prepare the synthetic wastewater feed solutions of copper, chromium, and mercury respectively. For chromium containing feed solution, the pH was adjusted to ~2.5 by adding 0.1 mol/L H_2SO_4 after dissolving the salt; for mercury feed solution, 0.1 mol/L HCl solution was used to dissolve mercuric chloride. Strip solutions were 2 mol/L H_2SO_4 (Fisher, Springfield, NJ) for Cu^{2+}, 0.5 mol/L NaOH (Fisher, Springfield, NJ) for Cr^{6+} and 1 mol/L NaOH in 4 mol/L NaCl (Aldrich, Milwaukee, WI) for Hg^{2+}. The salt was used to prevent formation of the precipitate in the alkaline media when mercury was concentrated in the strip solution. All chemicals were ACS reagent grade except TOA which was available at 95% purity.

Equilibrium distribution coefficient m_i of a metallic species i between the feed aqueous phase and the individual organic extractant is defined as:

$$m_i = \frac{\text{metal concentration of organic phase}}{\text{metal concentration of aqueous phase}} \tag{6}$$

Distribution coefficients were measured by stirring a known volume of the aqueous phase containing metal ion with an equal volume of the organic extractant and then separating out the aqueous and organic phases in a separating funnel. The aqueous phase concentration was measured; the organic-phase concentration was determined by material balance. In case of emulsion formation, the aqueous and the organic phases were separated in a centrifuge (Sorvall Model RC2-B, Newtown, CT) at 8,000 rpm for 15 min. In chromium extraction by TOA, the extraction reaction rate is quite fast; further a stable emulsion is formed when the two phases are mixed for longer time (more than 30 min) and TOA has a tendency to be oxidized by air. Therefore, distribution coefficient experiments for chromium were carried out for small contact time between the aqueous phase and the organic phase. Moreover, a high capacity centrifuge was used to break the emulsion after stirring.

A Perkin-Elmer 3030 AAS (Atomic Absorption Spectrophotometer) was used for measuring the concentration of Cu^{2+}, Cr^{6+}, and Hg^{2+} using individual Hollow Cathode Lamp. For Cu^{2+}, conventional flame condition with a fuel (acetylene) to air ratio of 15:45 was used. High concentration samples were diluted to the linear calibration range of 1 ~ 100 mg/L; measurements were made at 249.2 nm with a slit width of 0.7 nm. Very low concentration samples (< 5 mg/L) were measured at 325.2 nm using the same slit width which had a linearity up to 5 mg/L. The aqueous phase pH was measured using a Corning pH meter model 250 (relative accuracy = 0.001 pH error) obtained from Fisher Scientific (Springfield, NJ).

For Cr^{6+} concentration measurement by AAS, a linear calibration range of 0 ~ 7 mg/L was used at a wavelength of 359.4 nm and a slit width of 0.7 nm under conventional flame condition: the ratio of acetylene to air was 28:45. Measurement of feed outlet Cr^{6+} concentration (from actual runs in HFCLM permeator) was done in a similar manner using the AAS. Bausch and Lomb Spectrophotometer. Model 1001 was used to determine the strip side Cr^{6+} (in alkaline solution) concentration. Hg^{2+} was analyzed by AAS with a linear calibration range up to 300 mg/L at 253.7 nm and a slit width of 0.7 nm under conventional flame condition: the ratio of acetylene to air was 15:45. For high sensitivity determinations, a mercury/hydride system was used.

Table 1. Geometrical Characteristics of HFCLM Modules Used[#]

Module No.	Active Length cm	No. of 1st Fiber Set*	No. of 2nd Fiber Set*	Packing Density %	Effective Area/Vol. cm^{-1}
1**	48	300	300	36.3	64.5
2†	28	720	360	15.1	26.8
3‡	28	720	360	60.3	107.1
4†	24	600	600	16.7	29.8

* Microporous hollow fiber used (Celgard X-10, Hoechst Celanese, Charlotte, NC): ID = 100 μm; OD = 150 μm; fiber bubble point pressure = 1,034 kPa; porosity = 0.2; tortuosity = 3.5; mean pore size = 0.03 μm.

** Shell was made of a Teflon tube inserted into stainless steel outer shell (ID of Teflon tube = 0.61 cm).

† Shell was made of Teflon FEP tube: ID = 1.27 cm (Cole Parmer, Chicago, IL).

‡ Shell was made of glass: ID = 0.635 cm.

Modules 1, 2, 3, and 4 in this article correspond to permeators 1, 2, 3, and 5 (Yun, 1992).

Fabrication of HFCLM permeators

Detailed geometrical characteristics of four permeators fabricated are shown in Table 1. For Permeator #1, two sets of hollow fibers (Celgard X-10, 100 μm ID, 150 μm OD) were bundled, then placed inside a 0.61 cm ID Teflon sleeve located inside a 1.05 cm ID stainless steel pipe. The fibers were potted using Armstrong epoxies (Beacon Chemical Co., Mt. Vernon, NY), C4-D for internal tube sheet, and A2-A for external hardening. Complete curing of the resin required 7 days. Permeators #2 to #4 were somewhat different. Transparent Teflon FEP tube (1.27 cm ID and 1.43 cm OD) was used as shell along with polypropylene Y-fittings at two ends instead of a stainless steel pipe and Y-fittings used in Permeator #1. The transparent shell allowed the observation of any change in the membrane liquid during the simultaneous extraction and stripping process. To make a highly packed permeator, a glass insert (ID = 0.95 cm) was used in Permeator #3. In the fabrication of a highly packed HFCLM module, the mixing of two fiber sets was important to achieve a high module performance, since there was less space for movement by fibers swollen by the organic phase compared to that in a module with lower packing density. After a 7-d cure, the permeators were characterized for membrane thickness by gas permeation studies (Majumdar et al., 1989).

Removal and recovery of metals using HFCLM modules

Simultaneous removal and recovery of each toxic heavy metal were done separately using HFCLM modules (Permeators #1 to #3 for copper and Permeator #4 for chromium and mercury). A schematic of the experimental setup is shown in Figure 2. The setup had three components: feed line, strip line, and membrane liquid line all connected to the HFCLM module. Both aqueous phases flowed through the bore of two separate fiber sets concurrently and the organic extractant (the liquid membrane) was kept between these two fiber sets. Since the fibers were hydrophobic, the liquid membrane wetted the pores in the fiber wall; the phase interfaces were located at the inside wall of each fiber set by keeping the pressures of the aqueous phases slightly higher than that of the organic phase (there were two phase interfaces). The pressure difference between the aqueous phase and the organic phase was adjusted to 13.8 kPa at the outlet of both aqueous streams since the mode of operation was cocurrent and once-through.

To obtain steady-state flux, the system was allowed to run for 6 to 24 h in any experiment at particular feed and strip flow rates. Steady state was assured when three consecutive samples which were collected at a constant interval (every 2 h after 6 h running for Permeator #3, every 4 h after 24 h running for permeators #2 and #4, and every 6 h after 24 h running for Permeator #1) contained essentially the same concentration of the metal.

Modeling of Copper Transport

We have modeled Cu^{2+} transport through LIX 84 in *n*-heptane in a HFCLM permeator. Figure 1 describes the concentration profiles of different species in such a countertransport of Cu^{2+} and H^+ in the HFCLM configuration. Species in the organic liquid membrane phase are designated by an overbar. At the feed-liquid membrane interface, Cu^{2+} from the feed solution at a low H^+ concentration reacts with LIX

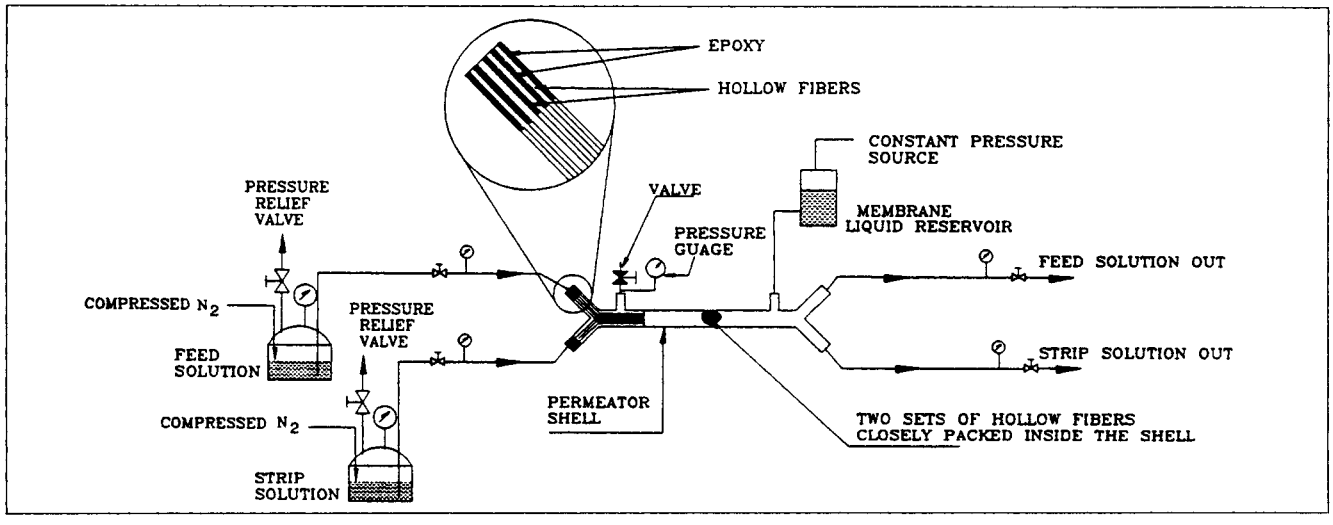

Figure 2. Experimental setup and a hollow fiber contained liquid membrane permeator.

84 and releases H^+, whereas at the strip-interface Cu^{2+} and LIX 84 are regenerated by H^+ from the strip solution according to Eq. 1. The equilibrium constant for this reaction may be written as:

$$K_{eq}=\frac{[\overline{R_2Cu}][H^+]^2}{[\overline{RH}]^2[Cu^{2+}]} \tag{7}$$

We will now obtain an expression for each transport/reaction step by determining R_T, the rate at which Cu^{2+} (or its equivalent from) is transferred per unit permeator length. Mass-transfer rate of Cu^{2+} per unit length through the feed side boundary layer is described by:

$$R_T=k_C^F([Cu^{2+}]_{Fb}-[Cu^{2+}]_{FI})\pi d_i^F N_F \tag{8}$$

The rate of formation of copper-oxime complex at the feed-liquid membrane interface is:

$$R_T=k_f\left([Cu^{2+}]_{FI}\frac{[\overline{RH}]_{FI}}{[\overline{H}^+]_{FI}}-\frac{1}{K_{eq}}\frac{[\overline{R_2Cu}]_{FI}[H^+]_{FI}}{[\overline{RH}]_{FI}}\right)\pi d_i^F N_F\epsilon^F \tag{9}$$

This expression is valid for oxime concentration greater than 0.012 mol/L (Komasawa and Otake, 1983). A similar expression was used by Haan et al. (1989) for extraction of Cu^{2+} by 20 wt. % LIX 84 in *n*-decane in a hollow fiber membrane extractor. The rate of diffusion of the copper-oxime complex through the membrane immobilized in the pores of the feed fiber wall is:

$$R_T=\frac{D_{R_2Cu}}{\delta_w^F}([\overline{R_2Cu}]_{FI}-[\overline{R_2Cu}]_{FO})\pi d_{lm}^F N_F \tag{10}$$

Here the effective thickness of diffusion path through the fiber wall of porosity ϵ^F and tortuosity τ^F is:

$$\delta_w^F=\frac{\tau^F(d_o^F-d_i^F)/2}{\epsilon^F} \tag{11}$$

The rate of diffusion of the complex through the liquid membrane from the outside surface of feed fiber to the outside surface of strip fiber is:

$$R_T=\frac{D_{R_2Cu}}{\delta_m}A_{lm}([\overline{R_2Cu}]_{FO}-[\overline{R_2Cu}]_{SO});$$

where

$$A_{lm}=\frac{(\pi d_o^F N_F-\pi d_o^S N_S)}{\ln[(\pi d_o^F N_F)/(\pi d_o^S N_S)]} \tag{12}$$

The rate of diffusion of the complex through the membrane immobilized in the strip fiber wall is:

$$R_T=\frac{D_{R_2Cu}}{\delta_w^S}([\overline{R_2Cu}]_{SO}-[\overline{R_2Cu}]_{SI})\pi d_{lm}^S N_S \tag{13}$$

where the effective thickness of the diffusion path through the strip fiber wall of porosity ϵ^S and tortuosity τ^S is:

$$\delta_w^S=\frac{\tau^S(d_o^S-d_i^S)/2}{\epsilon^S} \tag{14}$$

The rate of regeneration of copper at the strip side is:

$$R_T=k_r\left([\overline{R_2Cu}]_{SI}[H^+]_{SI}-K_{eq}\frac{[Cu^{2+}]_{SI}[\overline{RH}]_{SI}^2}{[H^+]_{SI}}\right)\pi d_i^S N_S\epsilon^S \tag{15}$$

Equations 9 and 15 were also used by Haan et al. (1989) for copper extraction and stripping by two membrane contactors. Teramoto and Tanimoto (1983) have used similar expressions for copper permeation through SME 529. The expressions for extraction and stripping were also verified by Yi and Tavlarides (1992) for copper permeation through LIX 84. The forward and reverse reaction rate constants obtained earlier by Haan et al. (1989) are close to the values obtained by Yi and Tavalrides (1992).

The mass-transfer rate of Cu^{2+} per unit permeator length through the strip side boundary layer is:

$$R_T=k_C^S([Cu^{2+}]_{SI}-[Cu^{2+}]_{Sb})\pi d_i^S N_S \tag{16}$$

Note that diffusional transfer of oxime occurs in the direction opposite to that of copper complex. The rate of diffusion of free oxime through the membrane immobilized in the pores of the feed fiber wall may be related to R_T by:

$$R_T=\frac{1}{2}\frac{D_{RH}}{\delta_w^F}([\overline{RH}]_{FO}-[\overline{RH}]_{FI})\pi d_{lm}^F N_F \tag{17}$$

The rate of diffusion of the oxime through the membrane from the outside surface of the strip fiber to the outside surface of feed fiber may be related to R_T by:

$$R_T=\frac{1}{2}\frac{D_{RH}}{\delta_m}A_{lm}([\overline{RH}]_{SO}-[\overline{RH}]_{FO}) \tag{18}$$

where A_{lm} has been defined in Eq. 12. The rate of diffusion of the oxime through the membrane immobilized in the strip fiber wall may be related to R_T by:

$$R_T=\frac{1}{2}\frac{D_{RH}}{\delta_w^S}([\overline{RH}]_{SI}-[\overline{RH}]_{SO})\pi d_{lm}^S N_S \tag{19}$$

Since hydrogen ion generated by the reactions at feed and strip interfaces has to diffuse through the respective boundary layers, the mass-transfer rate of hydrogen ion is related to R_T by:

$$\begin{aligned}R_T&=\frac{1}{2}k_H^F([H^+]_{FI}-[H^+]_{Fb})\pi d_i^F N_F\\&=\frac{1}{2}k_H^S([H^+]_{Sb}-[H^+]_{SI})\pi d_i^S N_S\end{aligned} \tag{20}$$

Define

$$k_f' = k_f \frac{[\overline{RH}]_{FI}}{[H^+]_{FI}};\quad k_r' = \frac{k_f}{K_{eq}} \frac{[H^+]_{FI}}{[\overline{RH}]_{FI}};$$

$$K_D' = \frac{k_r'}{k_f'} = \frac{[Cu^{2+}]_{FI}}{[\overline{R_2Cu}]_{FI}} = \frac{1}{m_C^F} \tag{21}$$

$$k_f'' = k_r K_{eq} \frac{[\overline{RH}]_{SI}^2}{[H^+]_{SI}};\quad k_r'' = k_r [H^+]_{SI};$$

$$K_D'' = \frac{k_r''}{k_f''} = \frac{[Cu^{2+}]_{SI}}{[\overline{R_2Cu}]_{SI}} = \frac{1}{m_C^S} \tag{22}$$

Assume now

$$d_i^F = d_i^S;\ d_o^F = d_o^S;\ \tau^F = \tau^S = \tau;\ \epsilon^F = \epsilon^S = \epsilon;\ \delta_w^F = \delta_w^S \tag{23}$$

Equations 8, 9, 10, 12, 13, 15, and 16 can be combined to get an expression for the rate of permeation of Cu^{2+} from the feed side to the strip side in case of unequal number of feed and strip fibers:

$$R_T = \pi d_i^F N_F \frac{\left([Cu^{2+}]_{Fb} - \frac{K_D'}{K_D''}[Cu^{2+}]_{Sb}\right)}{\left[\frac{1}{k_C^F} + \frac{\epsilon^{-1}}{k_f'} + \frac{K_D'}{D_{R_2Cu}/t_{eff}} + \frac{K_D'\epsilon^{-1}}{K_D'' k_f''}\frac{N_F}{N_S} + \frac{K_D'}{K_D'' k_C^S}\frac{N_F}{N_S}\right]} \tag{24}$$

where

$$t_{eff} = \frac{d_i}{d_{lm}} \frac{\tau(d_o - d_i)/2}{\epsilon}\left(1 + \frac{N_F}{N_S}\right) + \frac{\pi d_i N_F}{A_{lm}}\delta_m$$

For equal number of feed and strip fibers, diffusive transfer rate of the copper oxime complex through the liquid membrane can be expressed as:

$$R_T = \frac{D_{R_2Cu}}{t_{eff}}([\overline{R_2Cu}]_{FI} - [\overline{R_2Cu}]_{SI})\pi d_i^F N_F; \tag{25}$$

where

$$t_{eff} = \frac{d_i}{d_{lm}} \frac{\tau(d_o - d_i)}{\epsilon} + \frac{d_i}{d_o}\delta_m$$

Assuming equal diffusivities of both free oxime and complex

$$[\overline{RH}]_t = [\overline{RH}]_{FI} + 2[\overline{R_2Cu}]_{FI} = [\overline{RH}]_{SI} + 2[\overline{R_2Cu}]_{SI} = [\overline{RH}] + 2[\overline{R_2Cu}] \tag{26}$$

At steady state,

$$R_T = \pi d_i^F N_F \frac{\left([Cu^{2+}]_{Fb} - \frac{K_D'}{K_D''}[Cu^{2+}]_{Sb}\right)}{\left[\frac{1}{k_C^F} + \frac{\epsilon^{-1}}{k_f'} + \frac{K_D'}{D_{R_2Cu}/t_{eff}} + \frac{K_D'\epsilon^{-1}}{K_D'' k_f''} + \frac{K_D'}{K_D'' k_C^S}\right]} \tag{27}$$

If the distribution coefficient values are known corresponding to the feed and strip interfacial concentrations, they can be used directly to find out the local transfer rates.

Since we have maintained high H_2SO_4 concentrations at the strip side, concentration of copper-oxime complex at the strip aqueous-organic interface can be neglected. Therefore, copper transport rate/unit length through the membrane can be written as

$$R_T = \pi d_i^F N_F \frac{D_{R_2Cu}}{t_{eff}}[\overline{R_2Cu}]_{FI} = \frac{1}{2}\frac{D_{R_2Cu}}{t_{eff}}([\overline{RH}]_t - [\overline{RH}]_{FI})\pi d_i^F N_F \tag{28}$$

Several limiting R_T expressions for such a case are given below if a particular resistance controls:

Case #1. Aqueous film diffusion controls:

$$R_T = \pi d_i^F N_F k_C^F [Cu^{2+}]_{Fb} \tag{29}$$

Case #2. Membrane diffusion controls:

$$R_T = \pi d_i^F N_F \frac{D_{R_2Cu}}{t_{eff}}[\overline{R_2Cu}]_{FI} \tag{30}$$

Case #3. Interfacial reaction controls:

$$R_T = \pi d_i^F N_F k_f [Cu^{2+}]_{FI} \frac{[\overline{RH}]_{FI}}{[H^+]_{FI}}\epsilon \tag{31}$$

Assuming no controlling step:

$$R_T = \pi d_i^F N_F \frac{[Cu^{2+}]_{Fb}}{\left[\frac{1}{k_C^F} + \frac{\epsilon^{-1}}{k_f'} + \frac{K_D'}{D_{R_2Cu}/t_{eff}}\right]} \tag{32}$$

We can now write differential mass balances for Cu^{2+} and H^+ along the length of the permeator for both feed and strip sides as:

$$-Q_F \frac{d[Cu^{2+}]_{Fb}}{dz} = R_T;\quad Q_S \frac{d[Cu^{2+}]_{Sb}}{dz} = R_T \tag{33}$$

$$Q_F \frac{d[H^+]_{Fb}}{dz} = 2R_T;\quad -Q_S \frac{d[H^+]_{Sb}}{dz} = 2R_T \tag{34}$$

The aqueous side mass-transfer coefficients were calculated from the Graetz solution (Skelland, 1974) as:

$$N_{Sh} = 0.5 \frac{d_i}{L} N_{Re} N_{Sc} \theta$$

and

$$\theta = \frac{1 - \sum_{j=1}^{\infty} -4\frac{B_j}{\beta_j^2}\left(\frac{d\phi_j}{dr_+}\right)\Big|_{r_+=1} \exp\left[-\frac{\beta_j^2\left(2\frac{L}{d_i}\right)}{N_{Re}N_{Sc}}\right]}{1 + \sum_{j=1}^{\infty} -4\frac{B_j}{\beta_j^2}\left(\frac{d\phi_j}{dr_+}\right)\Big|_{r_+=1} \exp\left[-\frac{\beta_j^2\left(2\frac{L}{d_i}\right)}{N_{Re}N_{Sc}}\right]} \quad (35)$$

where

$$\beta_j = 4(j-1) + \frac{8}{3}; \quad -\frac{1}{2}B_j\left(\frac{d\phi_j}{dr_+}\right)\Big|_{r_+=1} = 1.01276\beta_j^{-1/3};$$

$$j = 1, 2, 3$$

Define the following nondimensional variables:

$$q_1 = Q_F/Q_{\text{ref}}; \; q_2 = Q_S/Q_{\text{ref}}; \; C_1 = [Cu^{2+}]_{Fb}/C_{\text{ref}};$$
$$C_2 = [Cu^{2+}]_{Sb}/C_{\text{ref}}; \; C_3 = [H^+]_{Fb}/C_{\text{ref}}; \; C_4 = [H^+]_{Sb}/C_{\text{ref}};$$
$$\overline{C_M} = [\overline{RH}]/[\overline{RH}]_t; \; S = \frac{1}{2}\frac{\pi d_i^F N_F}{Q_{\text{ref}}}\frac{D_{R_2Cu}}{t_{\text{eff}}}\frac{[\overline{RH}]_t}{C_{\text{ref}}}l\zeta; \quad (36)$$

where $C_{\text{ref}} = [Cu^{2+}]_{Fb}$ at $z = 0$, that is, inlet feed Cu^{2+} concentration; $\zeta = z/l$. Using expression of R_T from Eq. 29 when boundary layer resistance controls permeation, Eqs. 33 and 34 in the dimensionless form can be written as:

$$-q_1\frac{dC_1}{dS} = 2\frac{C_{\text{ref}}}{[\overline{RH}]_t}\frac{k_C^F}{\frac{D_{R_2Cu}}{t_{\text{eff}}}}C_1 = q_2\frac{dC_2}{dS} \quad (37)$$

$$q_1\frac{dC_3}{dS} = 4\frac{C_{\text{ref}}}{[\overline{RH}]_t}\frac{k_C^F}{\frac{D_{R_2Cu}}{t_{\text{eff}}}}C_1 = -q_2\frac{dC_4}{dS} \quad (38)$$

Using Eq. 28 in the case of all other controlling steps, Eq. 33 and Eq. 34 in the dimensionless form can be written as:

$$-q_1\frac{dC_1}{dS} = [1 - \overline{C_M}] = q_2\frac{dC_2}{dS} \quad (39)$$

$$q_1\frac{dC_3}{dS} = 2[1 - \overline{C_M}] = -q_2\frac{dC_4}{dS} \quad (40)$$

where expressions for $\overline{C_M}$ differ depending on the individual controlling resistances. When interfacial reaction rate controls the transport, by combining Eq. 31 and Eq. 28, $\overline{C_M}$ can be expressed as:

$$\overline{C_M} = \epsilon\frac{\frac{D_{R_2Cu}}{t_{\text{eff}}}}{2k_f\frac{C_1}{C_3} + \frac{D_{R_2Cu}}{t_{\text{eff}}}} \quad (41)$$

If the diffusional resistance through the liquid membrane controls the transport, by combining Eqs. 7, 30 and 28, $\overline{C_M}$ can be expressed as:

$$\overline{C_M} = \frac{-1 + (1 + 8\alpha)^{1/2}}{4\alpha} \quad (42)$$

where

$$\alpha = K_{\text{eq}}\frac{[\overline{RH}]_t}{C_{\text{ref}}}\frac{C_1}{C_3^2} \quad (43)$$

When all resistances control the transport, by combining Eqs. 32 and 28 the dimensionless oxime concentration can be obtained from:

$$\overline{C_M}^3 + \alpha_1\overline{C_M}^2 + \alpha_2\overline{C_M} + \alpha_3 = 0 \quad (44)$$

where

$$\alpha_1 = \frac{C_{\text{ref}}}{[\overline{RH}]_t}\left[\frac{2C_1k_C^F}{\frac{D_{R_2Cu}}{t_{\text{eff}}}} + C_3\frac{k_C^F}{k_f\epsilon}\right] - 1;$$

$$\alpha_2 = \frac{C_{\text{ref}}}{[\overline{RH}]_t}\left[\frac{C_3^2}{K_{\text{eq}}}\frac{C_{\text{ref}}}{[\overline{RH}]_t}\frac{k_C^F}{\frac{D_{R_2Cu}}{t_{\text{eff}}}} - C_3\frac{k_C^F}{k_f\epsilon}\right];$$

$$\alpha_3 = -\frac{C_3^2}{K_{\text{eq}}}\frac{k_C^F}{\frac{D_{R_2Cu}}{t_{\text{eff}}}}\frac{C_{\text{ref}}^2}{[\overline{RH}]_t^2} \quad (45)$$

Results and Discussion

We will present first the values of the distribution coefficients (m_i) and then illustrate the separation/concentration for Cr^{6+} and Hg^{2+} in a HFCLM permeator. We will present next in detail a variety of results of separation/concentration of Cu^{2+} in different types of HFCLM permeators. Finally, we explore how well the model developed here predicts the separation-concentration behavior for Cu^{2+} in such novel HFCLM permeators.

Distribution coefficients

The experimental values of the equilibrium distribution coefficient of chromium (as Cr^{6+}) in 20 v/v % TOA in xylene (without any modifier) as a function of the aqueous phase Cr^{6+} concentration are presented in Table 2. The pH values of the aqueous phase before mixing with the organic phase and after equilibrium are also indicated. The distribution coefficient shows a maxima up to a certain initial concentration followed by a decreasing trend. This could be attributed to a deficiency in H^+ concentration at higher initial feed Cr^{6+} concentrations. According to reaction 2, 52 mg/L of Cr^{6+} requires 1 mg/L of H^+ ion. A pH of 2.5 corresponds to 3.2 mg/L of H^+ ion in the solution. As the initial Cr^{6+} concentration increases, demand for H^+ also increases resulting in the lower amount of

Table 2. Distribution Coefficient of Cr^{6+} with 20 v/v % TOA in Xylene

Starting Aqueous Phase		Aqueous Phase after Equilibrium		
Cr^{6+} Conc. mg/L	pH	Cr^{6+} Conc. mg/L	pH	m_i
450	2.42	112.7	5.71	2.99
400	2.48	117.5	5.72	2.40
350	2.45	64.2	5.53	4.45
300	2.36	8.8	4.28	33.09
200	2.51	10.8	3.55	17.37
99	2.50	6.4	—	14.43
75	2.46	5.6	3.42	12.38
50	2.39	4.4	3.34	10.21
25	2.50	2.3	3.25	9.68
10	2.43	1.8	3.19	4.32

complexation with TOA, thereby decreasing the distribution coefficient at higher levels of Cr^{6+} concentration. This trend can be reversed by adding more H_2SO_4 into the aqueous phase.

The experimental values of equilibrium distribution coefficient of Hg^{2+} in 20% v/v TOA in xylene as a function of the aqueous phase Hg^{2+} concentration are presented in Table 3. The pH values of the aqueous phase after mixing with the organic phase are also indicated. Much lower values for higher concentrations were mainly due to much lower initial HCl concentration in the system as is evident from reaction 4. Similar trends were observed earlier in literature (Caban and Chapman, 1972). We are not presenting here the information on Cu^{2+} distribution coefficients at different concentrations of LIX 84 in *n*-heptane. The results are available in Yun (1992) and Yun et al. (1993). They have utilized the following relation between the equilibrium constant K_{eq} (defined by Eq. 7) for reaction 1, the distribution coefficient m_i (defined by Eq. 6), the pH, and the chelating agent concentration in the organic phase:

$$\log m_i = \log K_{eq} + 2 \log \frac{[\overline{RH}]}{[H^+]} \qquad (46)$$

They have further obtained the value of K_{eq} as 1.7 from the m_i data (described by an appropriate regression equation for each LIX 84 concentration) for the system of reaction 1. We have used this value of K_{eq} for all of our model calculations.

HFCLM permeator performance

Removal/Concentration of Cr^{6+} and Hg^{2+}. Steady-state

Table 3. Distribution Coefficient of Hg^{2+} with 20 v/v % TOA in Xylene

Initial Aqueous Phase Hg^{2+} Conc., mg/L	Equilibrium Aqueous Phase Hg^{2+} Conc., mg/L	m_i	pH
20,000	5,665	2.5	5.98
15,000	2,192.5	5.8	5.98
10,000	249.4	39.1	4.71
5,000	3.7	1,350.4	3.68

Notes: (1) Initial organic phase composition = 20 v/v % TOA in xylene.
(2) Initial HCl concentration of aqueous phase = 0.1 mol/L.

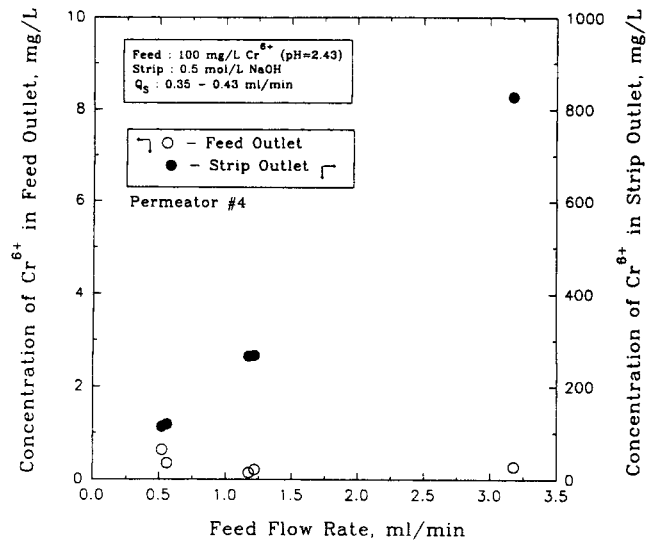

Figure 3. Effect of feed flow variation on feed and strip outlet concentrations of chromium for permeator #4.

Concentration of chromium in feed inlet = 100 mg/L; liquid membrane = 20% v/v TOA in xylene with 5% v/v 2-ethyl-1-hexanol as a modifier.

data for the removal and concentration of Cr^{6+} in Permeator #4 for different feed concentrations and feed flow rates are shown in Figures 3 and 4. A low strip flow rate (up to 20 times lower than the feed flow rate) was maintained to remove Cr^{6+} from the feed and simultaneously enrich it in the strip side. These results suggest that Cr^{6+} in the feed wastewater (100 mg/L, pH = 2.43) can be reduced to less than 1 mg/L as it was simultaneously concentrated to about 800 mg/L in strip side (Figure 3); similarly 250 mg/L Cr^{6+} feed (pH = 2.5) was

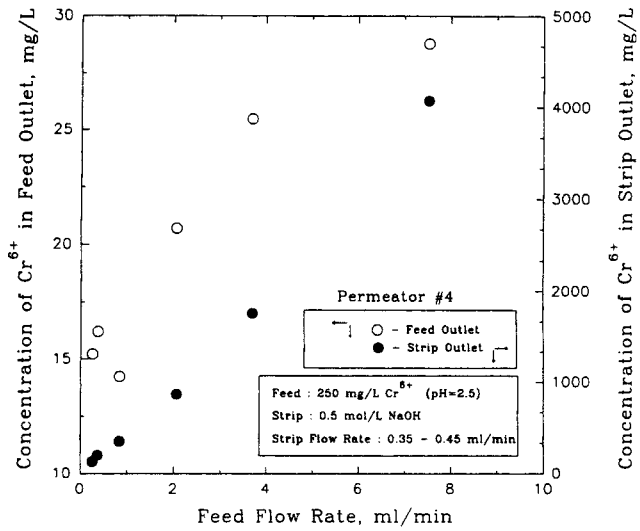

Figure 4. Effect of feed flow variation on feed and strip outlet concentrations of chromium for permeator #4.

Concentration of chromium in feed inlet = 250 mg/L; liquid membrane = 20% v/v TOA in xylene with 5% v/v 2-ethyl-1-hexanol as a modifier.

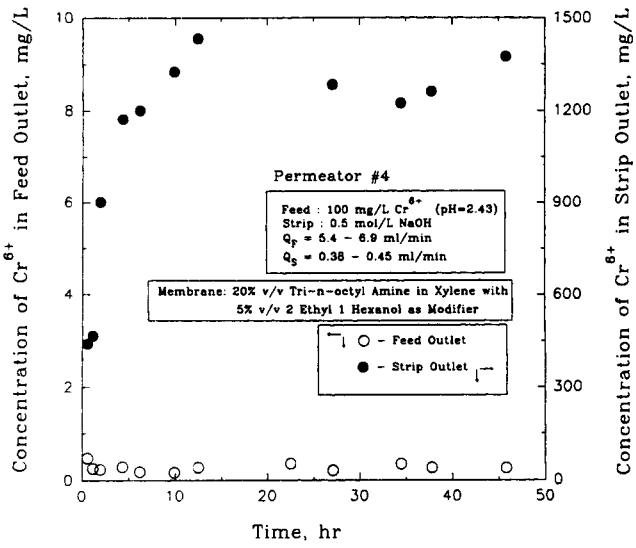

Figure 5. 50 h run for Cr^{6+} removal and recovery in permeator #4.

Concentration of chromium in feed inlet = 250 mg/L; liquid membrane = 20% v/v TOA in xylene with 5% v/v 2-ethyl-1-hexanol as a modifier.

reduced to less than 30 mg/L with 16 times enrichment in strip side to around 4,000 mg/L (Figure 4). Had we provided more membrane area, we could have easily reduced the outlet concentration from 30 to 1 mg/L or lower

Results of a 50-h run are shown in Figure 5. Strip outlet concentration fluctuations were due to changes in feed flow rates. During this 50-h run, a brownish precipitate was observed in the strip side. Similar precipitation in the liquid membrane was reported by Pearson (1983). The precipitate was dissolved in 2 mol/L H_2SO_4 solution. By slowly circulating the liquid membrane through a filter present outside of the module, the accumulation of the precipitate in the liquid membrane may be prevented for steady performance over a long period. In actual operation, such a precipitate may be flushed out easily by increasing the strip flow rate drastically for a short period of time. This strip solution can then be filtered outside and recirculated back to the strip inlet.

Results of removal and concentration of Hg^{2+} using Permeator #4 are shown in Figure 6. Starting from a feed inlet concentration around 200 mg/L, a feed outlet concentration of about 4×10^{-3} mg/L was attained with simultaneous Hg^{2+} concentration of about 2,150 mg/L in the strip side illustrating the high efficiency and selectivity of the process. During this experiment, the pressure of the strip outlet dropped slowly due to the deposition of some precipitate in the strip side wall (the strip side flow rate decreased from 0.91 to 0.48 mL/min). This deposit had an orange color and appeared in significant quantities when the feed flow rate was high. After this experiment, the deposit was completely removed by backflushing with 0.1 mol/L HCl solution. This precipitate can also be removed by the strip flushing method described earlier.

Removal/Concentration of Cu^{2+}. The results of copper removal/concentration are reported next. Since the objective was to purify the feed solution by removing Cu^{2+} and to simultaneously enrich Cu^{2+} in the strip side to the maximum extent, the strip flow rate should be kept much lower than the feed flow rate whose variation was studied using Permeator #1. Experiments were carried out with initial Cu^{2+} concentrations varying between 91-385 mg/L. Figure 7 shows the results with a low feed inlet copper concentration (~91 mg/L Cu^{2+}) and a not-too-low strip flow rate. Feed outlet copper concentration was less than 2 mg/L and at low feed flow rates, values as low as 0.1 mg/L were achieved. High enrichment was not achieved as the strip flow rate was not significantly lower than that of the feed side.

To study the effect of extractant concentration, experiments were done next with different LIX 84 concentrations in *n*-heptane. Effects of different feed flow rates for successful

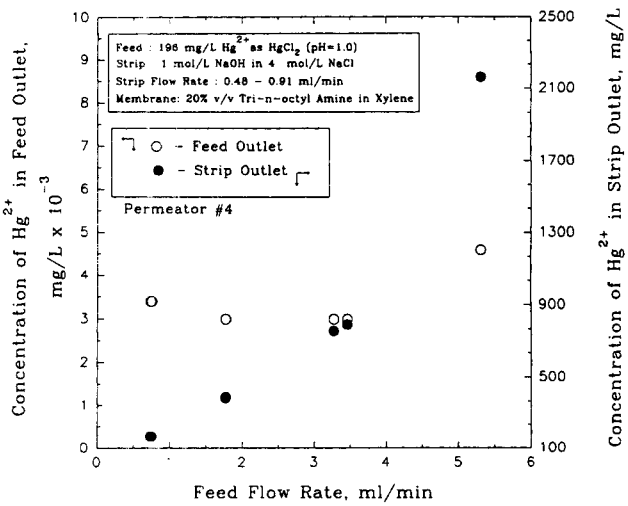

Figure 6. Effect of feed flow variation on feed and strip outlet concentrations of mercury for permeator #4.

Concentration of mercury in feed inlet = 196 mg/L; liquid membrane = 20% v/v TOA in xylene.

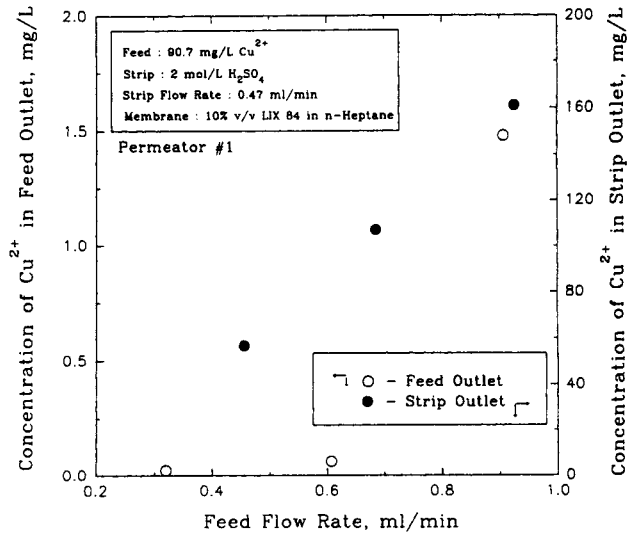

Figure 7. Effect of feed flow variation on feed and strip outlet concentrations of copper for permeator #1.

Concentration of copper in feed inlet = 90.7 mg/L; liquid membrane = 10% v/v LIX 84 in *n*-heptane.

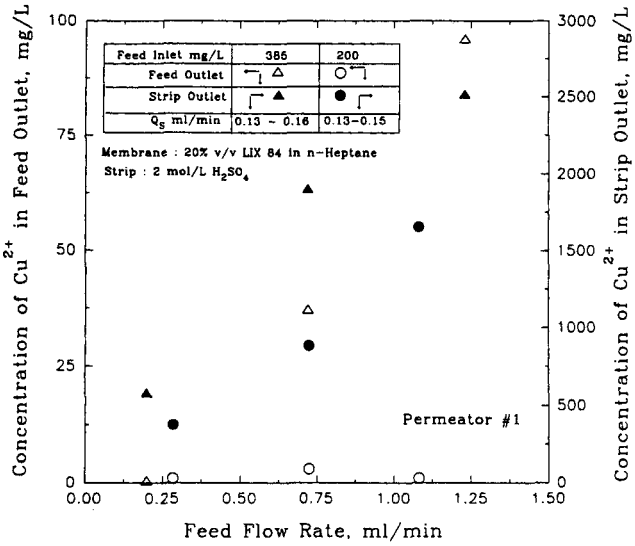

Figure 8. Effect of feed flow variation on feed and strip outlet concentrations of copper for permeator #1.

Concentrations of copper in feed inlet = 200 mg/L and 385 mg/L, respectively; liquid membrane = 20% v/v LIX 84 in *n*-heptane.

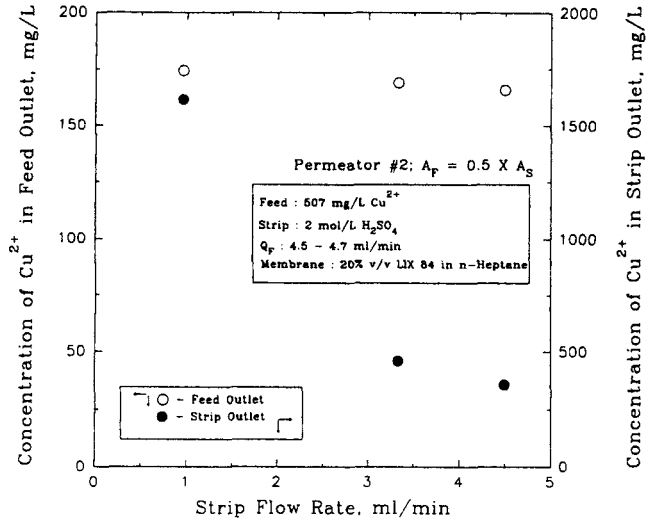

Figure 10. Effect of strip flow variation on feed and strip outlet concentrations of copper for permeator #2.

Concentration of copper in feed inlet = 507 mg/L; liquid membrane = 20% v/v LIX 84 in *n*-heptane; feed side area = 0.5 × strip side area.

removal of Cu^{2+} using 20% v/v LIX 84 as membrane are shown in Figure 8 where two different initial feed Cu^{2+} concentrations 200 mg/L and 385 mg/L were used. Only steady-state data are shown. When feed inlet Cu^{2+} concentration was 200 mg/L, outlet concentration was brought down to less than 2 mg/L while Cu^{2+} was concentrated in the strip side up to 1,700 m/L. When feed inlet Cu^{2+} concentration was 385 mg/L outlet concentration was brought down to 96 mg/L while Cu^{2+} was concentrated in the strip side up to 2,520 mg/L for a high feed flow rate. At a lower feed flow rate the feed outlet concentration was brought down to around 4 mg/L. These data show that a very high level of Cu^{2+} removal was easily achieved at low aqueous flow rates in a given permeator. This also implies that, by providing proportionately more membrane area, the feed outlet concentration can be reduced to a very low value and at the same time Cu^{2+} can be concentrated to a much higher level in the strip side. Therefore, successful removal and concentration of Cu^{2+} from an aqueous waste stream is feasible using LIX 84 as the complexing extractant in the liquid membrane in a HFCLM permeator.

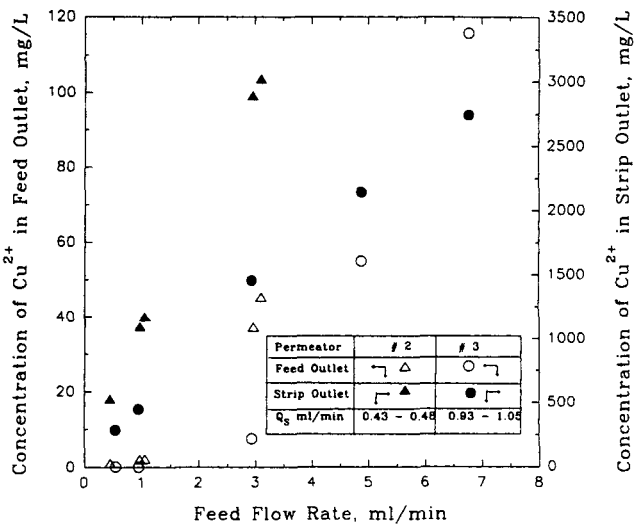

Figure 9. Effect of feed flow variation on feed and strip outlet concentrations of copper with permeators #2 and #3.

Concentration of copper in feed inlet = 507 mg/L; liquid membrane = 20% v/v LIX 84 in *n*-heptane; feed side area = 2.0 × strip side area.

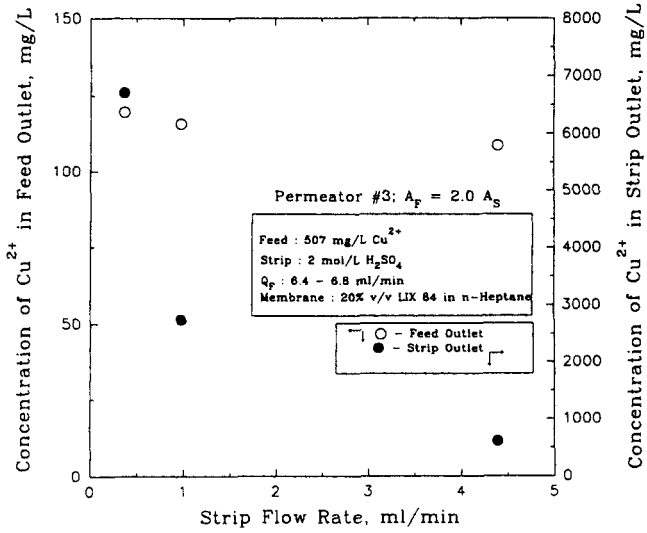

Figure 11. Effect of strip flow variation on feed and strip outlet concentrations of copper with permeator #3.

Concentration of copper in feed inlet = 507 mg/L; liquid membrane = 20% v/v LIX 84 in *n*-heptane; feed side area = 2.0 × strip side area.

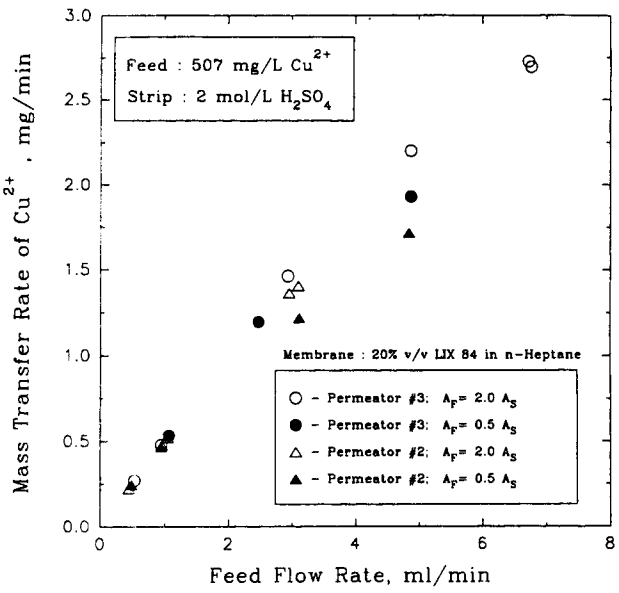

Figure 12. Effect of feed flow variation on mass-transfer rate of copper in different modules.

Concentration of copper in feed inlet = 507 mg/L; liquid membrane = 20% v/v LIX 84 in *n*-heptane.

Permeators #2 and #3 had different numbers of fibers in each set of fibers: one set had twice the number of fibers than that in the other. Therefore, depending on the flow path selected for a particular stream, such as feed or strip aqueous stream, the interfacial areas will be different. The effect of feed flow variations on feed and strip outlet concentrations in Permeators #2 and #3 are shown in Figure 9; the feed side area was twice that of the strip side area in both cases. Effects of strip flow variations on feed and strip outlet concentrations in such modules are shown in Figures 10 and 11 where feed side area was twice that of strip side area in the case of Permeator #3 (Figure 11) whereas feed side area was half of that of the strip side in case of Permeator #2 (Figure 10). The results indicate that strip side flow rate has no effect on the overall transport rate of Cu^{2+} through LIX 84 for these parametric variations. However, very high Cu^{2+} enrichment in the strip was possible (Figure 11 shows more than 13 times enrichment in the strip outlet stream to a level of 7,000 mg/L) as the strip side flow rate was reduced considerably.

Figure 12 shows the effects of feed flow variations on mass-transfer rate of Cu^{2+} in different interfacial area combinations obtained by switching feed and strip sides in a given module. These results indicate that, under otherwise identical conditions in a module, a higher flux was achieved when the feed side area was twice that of the strip side area. This suggests that the interfacial reaction resistance of the feed side is quite influential in Cu^{2+} transfer. The highest mass-transfer rate was achieved in module 3 when the feed side area was twice that of the strip side area.

Mass transport of copper from the feed solution to the strip solution is dependent on three types of resistances: boundary layer resistances on the feed side and the strip side; diffusional resistances of the free carrier and the complex through the contained liquid membrane including those in the pores of the membrane substrate; and resistances due to interfacial reactions at the feed and the strip interfaces. Since the concentration of H_2SO_4 in the strip side was maintained at a high level, strip aqueous phase flow rates did not affect the performance of copper transport through LIX 84 as shown in Figures 10 and 11. Therefore, the remaining resistances are due either to the feed aqueous side boundary layer or the diffusion through the liquid membrane or the reactions at the phase interfaces or a combination of these. Suppose the interfacial extraction reaction rate controls the overall transport rate of Cu^{2+} through LIX 84; a higher mass-transfer rate will be achieved then in a given module if the feed interfacial area is made larger than that in the strip side. This is so since the feed wastewater contained a low concentration of Cu^{2+} and a high H_2SO_4 concentration was maintained on the strip side (the reaction at the strip interface may be considered instantaneous).

Table 4. Parameters Used for Simulation

Parameter	Value
$D_{Cu^{2+}}$	7.2×10^{-6} cm^2/s*
D_{R_2Cu}	1.46×10^{-6} cm^2/s**
D_{H^+}	6.0×10^{-5} cm^2/s*
K_{eq}	1.7*
ϵk_f	9.0×10^{-8} m/s*
k_r	1.5×10^{-10} m^4/s·mol**
δ_m (Permeator #1)	76.2† μm
t_{eff} (based on Eq. 25)	760.2 μm
δ_m (Permeators #2 and #3)	40† μm
t_{eff} (based on Eq. 24; $N_F = 0.5\ N_S$)	555 μm
t_{eff} (based on Eq. 24; $N_F = 2\ N_S$)	1,100 μm

* Yun et al. (1993).
** Haan et al. (1989).
† Majumdar et al. (1988).

Numerical integration was carried out along the permeator length for both feed and strip sides with known initial concentrations assuming different rate controlling steps for the local flux expressions. Parameters used for simulation are listed in Table 4. Effective thickness, t_{eff}, was calculated for individual modules using substrate (hollow fiber wall) porosity as 0.2 and tortuosity as 3.5. Diffusivity and backward reaction rate constant values reported by Haan et al. (1989) were used for simulation. Values for the forward reaction rate constant and reaction equilibrium constant were obtained from extraction studies and experimental distribution coefficient values (Yun et al., 1993).

Experimental data were compared with the numerical simulation results shown in Figures 13–16. For low feed concentrations of 200–500 mg/L utilized in Figures 13–16 (obtained from Figures 8, 9, and 12), the resistance to diffusion through the liquid membrane is very low compared to that through the feed aqueous boundary layer and the resistance due to interfacial extraction reaction. The mass-transfer rate, obtained from the model, is much higher when membrane diffusion controls permeation. We have not reported these values in the individual figures. (Obviously, the role of diffusion resistance will change if feed copper concentration is much higher (O'Hara and Bohrer, 1989).) Moreover, for the feed flow regimes and concentration levels used here, the simulated outlet copper concentration becomes zero at some axial location of the module and integration along the whole permeator length then becomes redundant.

Simulation results in Figures 13 and 14 suggest that values

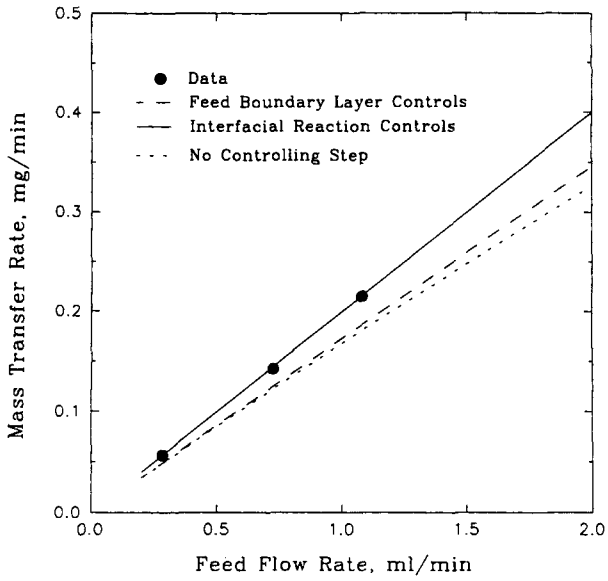

Figure 13. Comparison of experimental data with simulation results when the feed inlet concentration of copper was 200 mg/L.

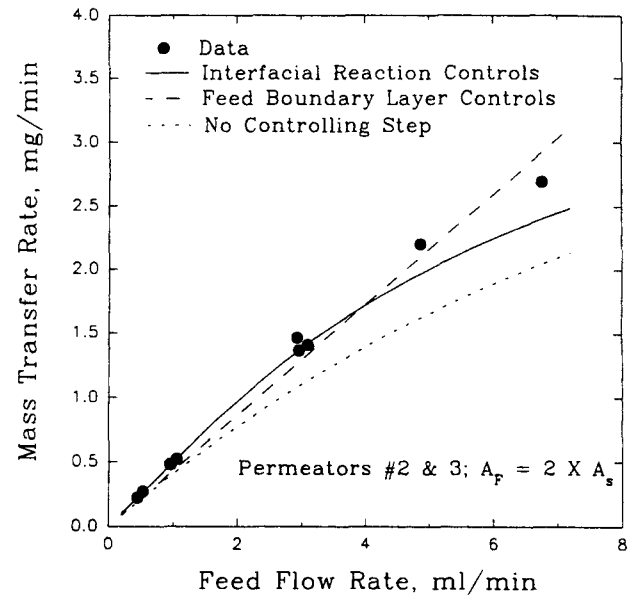

Figure 15. Comparison of experimental data with simulation results when the feed inlet concentration of copper was 500 mg/L and feed side area was twice the strip side area.

of mass-transfer rate at different flow rates based on no controlling step are closer to those values when feed boundary layer controls copper permeation. However, experimental data in Figure 13 were explained quite well using the model based on interfacial reaction-controlled permeation of Cu^{2+}. On the other hand in Figure 14, experimental data for a higher Cu^{2+} feed concentration (385 mg/L) were closer to the simulation results based on no controlling step. This is also true at low feed flow rates as shown in Figures 15 and 16. Simulation results in all these cases suggest that mass-transfer rate increases linearly with the feed flow rate when boundary layer resistance controls the permeation. However, this linearity with flow rate is not observed in the simulation results when interfacial reaction controls. The experimental data at higher flow rates show a trend similar to that for interfacial reaction controlled permeation in Figures 15 and 16. Therefore, comparing the numerical simulation results and the experimental data in Figures 15 and 16, it appears that at higher flow rates where boundary layer resistance becomes less important, interfacial reaction is the most likely rate controlling step for copper

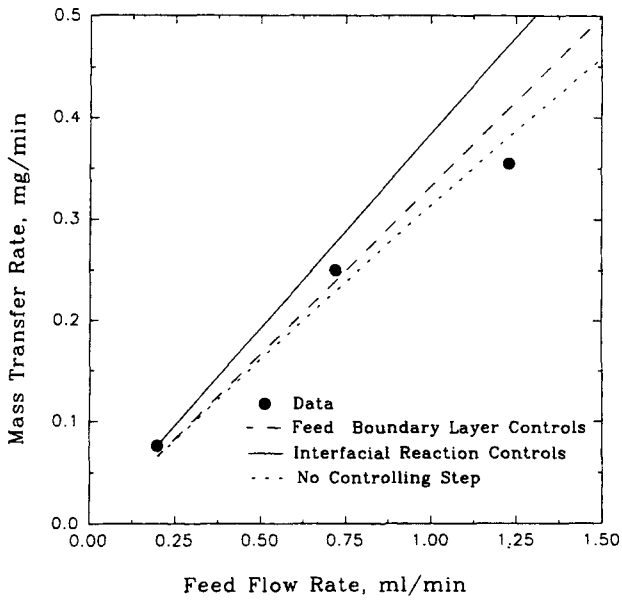

Figure 14. Comparison of experimental data with simulation results when the feed inlet concentration of copper was 385 mg/L.

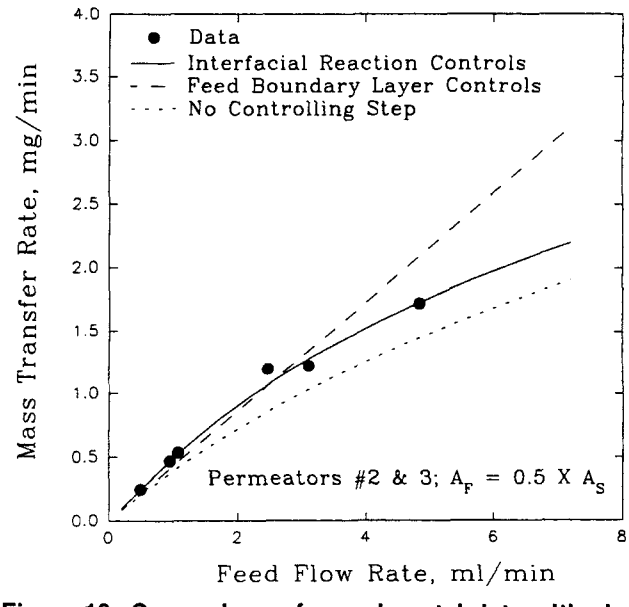

Figure 16. Comparison of experimental data with simulation results when the feed inlet concentration of copper was 500 mg/L and feed side area was half of the strip side area.

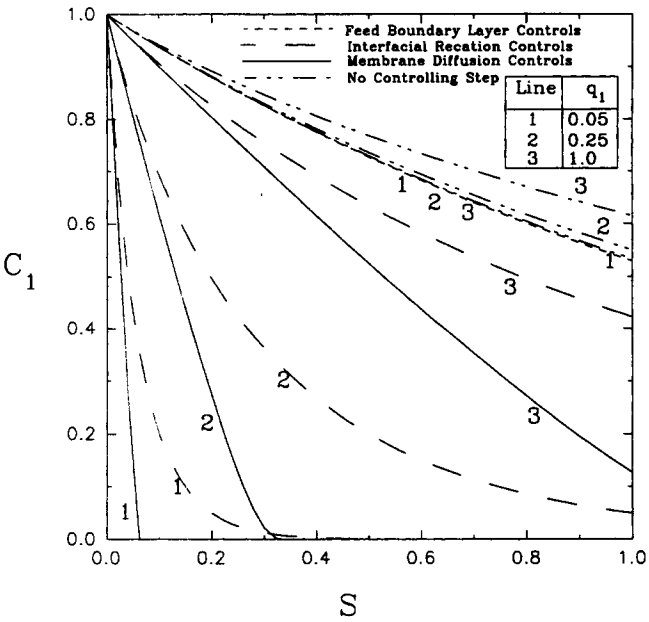

Figure 17. Simulated dimensionless concentration profiles of Cu^{2+} vs. dimensionless membrane area at different dimensionless feed flow rates assuming different controlling permeation steps.

Following parameters were used for different plots: $D_{R_2Cu} = 1.46 \times 10^{-6}$ cm^2/s, $[\overline{RH}]_i = 0.312$ mol/L, $N_F = 720$, $N_S = 360$, $t_{eff} = 1{,}100$ μm, $l = 28$ cm, $C_{ref} = 500$ mg/L.

transport through a liquid membrane containing LIX 84 in *n*-heptane.

In order to design any membrane module for the removal of Cu^{2+} or any other heavy metal, the main objective should be to maximize the utilization of the membrane area. Figure 17 shows simulated dimensionless concentration profiles of Cu^{2+} at different values of dimensionless membrane area S (defined by Eq. 36) for different values of the dimensionless feed flow rate q_1. The plots are based on the different rate controlling steps for permeation. Note that for a particular value of number of feed fibers (N_F), membrane thickness (t_{eff}), length of the module (l), diffusivity of the complex through the liquid membrane (D_{R_2Cu}), initial oxime concentration in the liquid membrane ($[\overline{RH}]_i$), and reference feed concentration (C_{ref}), the Q_{ref} in Eq. 36 can be chosen such that the value of S always lies between 0 and 1. Thus, for a given liquid membrane composition, one can vary N_F, t_{eff}, l, and C_{ref} without changing the profiles of C_1 vs. S as long as identical dimensionless flow rates were chosen. Note further that different numbers of feed and strip side fibers will affect the effective liquid membrane diffusion thickness from feed aqueous-organic interface to strip aqueous-organic interface according to Eq. 24. In the present case, when the number of feed fibers are twice that of strip fibers ($N_F = 720$ and $N_S = 360$), t_{eff} is 1,100 μm when $\delta_m = 40$ μm (Table 4). Contrary to this when the number of feed fibers is half that of strip fibers ($N_F = 360$ and $N_S = 720$) t_{eff} is 555 μm when $\delta_m = 40$ μm. However the simulation results will not change as long as the value of q_1 remains constant. If one wants to maximize the use of area in such a module, one should design the system so that the profile lies between lines 1 and 2 when interfacial reaction controls and between lines 2 and 3 when liquid membrane diffusion controls the permeation. If the transport is governed by diffusion through feed aqueous boundary layer, there is only one profile. This is evident from Eq. 37 and Eq. 38 if the boundary layer mass-transfer coefficient varies linearly with feed aqueous phase velocity according to Eq. 35 (when contribution of Θ approaches 1). When all the resistances are present the simulated profiles were dominated by boundary layer resistance for low q_1 (line 1) and as the value of q_1 increases, other resistances start to play their roles as evident from lines 2 and 3.

The model proposed here is based on steady state, that is, the liquid membrane composition is unaffected by time. We have studied Cu removal-concentration by a HFCLM permeator for extended periods of time. Such data for runs as long as one month or longer (Basu, 1990; Yun 1992) and appropriate models (Yun, 1992) will be presented in a future communication (Yun et al., 1994). It is noteworthy to mention that any loss of liquid membrane constituents to the aqueous feed and strip streams is countered by continuous and automatic addition from the membrane liquid reservoir. If there is an unbalance in this process there will be a slow change in the liquid membrane composition. However, such a slow change may not affect permeator performance over a long time. Strategies to counter such slow changes, if any, and the corresponding results will be presented in the future (Yun et al., 1994).

Conclusions

Heavy metals like Cu^{2+}, Cr^{6+}, and Hg^{2+} have been successfully removed from wastewater and concentrated in a strip aqueous solution in a HFCLM permeator. Using cotransport, Cr^{6+} from a dilute $K_2Cr_2O_7$ solution acidified with H_2SO_4 was transferred through a liquid membrane containing tri-*n*-octylamine in xylene and concentrated in an alkaline solution on the strip side. Feed solution was brought down to 0.5 mg/L level from 100 mg/L level as the strip solution was enriched to a high level. Employing the same liquid membrane, a 200 mg/L Hg^{2+} containing feed solution was brought down to 0.004 mg/L level. For Cu^{2+} extraction-concentration by countertransport using LIX 84 in *n*-heptane as the liquid membrane, a feed solution containing 500 mg/L of copper was brought down to 0.05 mg/L; simultaneously copper was concentrated up to 6,800 ppm in an acidic strip solution using appropriate feed and strip solution flow rates. Variations of strip flow rates indicated no effect on the permeation of copper.

A theoretical model has been developed for the permeation of copper through LIX 84 in *n*-heptane from the feed solution to the strip solution. For the lower feed concentration of 200 mg/L Cu^{2+}, the data agree well with the model where interfacial extraction reaction controls the permeation. As the concentration of feed solution was increased to 385 mg/L the model suggests that both aqueous boundary layer resistance and the resistance due to interfacial extraction reaction affect Cu^{2+} permeation. When the Cu^{2+} concentration was increased further to 500 mg/L, the resistance due to interfacial reaction at lower feed flow rates where boundary layer resistance dominates copper permeation was reduced by providing a higher feed side area as evident from the total mass-transfer rate.

However, an increase in feed flow rate decreased the resistance due to the feed boundary layer and the resistance due to interfacial reaction becomes dominant. On the other hand when the feed interfacial area is lower than the strip interfacial area, the effect of resistance due to interfacial reaction becomes prominent even at lower feed flow rates.

In such permeation processes where resistances like feed aqueous boundary layer and interfacial reaction play a dominant role, permeation rate can be increased either by increasing the feed flow rate or increasing the feed-side interfacial area. Thus, for a given flow rate the design parameters should be optimized by providing higher feed-side interfacial area, so that the resistance due to interfacial reaction does not supersede the boundary layer resistance. Ideally, the system should be operated in such a way that one can take advantage of higher interfacial area as well as lower boundary layer resistance to achieve the maximum mass-transfer rate of copper for a given membrane area. This is demonstrated here by varying the number of feed fibers vis-a-vis strip fibers. No existing liquid membrane technique other than HFCLM provides this flexibility.

Acknowledgment

We would like to acknowledge the research funds provided for this project by the EPA Northeast Hazardous Substance Research Center at NJIT, Newark, NJ. We express our thanks to Hoechst Celanese SPD, Charlotte, NC for providing hollow fibers and to Henkel, Tucson, AZ for providing LIX 84. The mercury/hydride system facility was made available to us by John Wiencek, Rutgers University, New Brunswick, NJ.

Notation

A_F = feed side interfacial area, $\pi d_i^F N_F$
A_{lm} = logarithmic mean area defined in Eq. 12
A_S = strip side interfacial area, $\pi d_i^S N_S$
C_1, C_2, C_3, C_4 = dimensionless concentrations defined in Eq. 36
$\overline{C_M}$ = dimensionless oxime concentration defined in Eq. 36
C_{ref} = aqueous feed inlet concentration of copper, mol/L
$[Cu^{2+}]$ = concentration of copper in the aqueous phase, mol/L
d_i^F, d_i^S = inner diameter of a feed and strip fiber, respectively, cm
d_o^F, d_o^S = outer diameter of a feed and strip fiber, respectively, cm
d_{lm}^F, d_{lm}^S = logarithmic mean diameter of a feed and strip fiber, respectively, cm
D_{RH} = diffusion coefficient of oxime in organic phase, cm^2/s
D_{R_2Cu} = diffusion coefficient of copper-complex in organic phase, cm^2/s
D_{iw} = diffusion coefficient of species i in aqueous phase, cm^2/s
$[H^+]$ = concentration of hydrogen ion in the aqueous phase, mol/L
k_i^F, k_i^S = feed and strip side boundary layer mass-transfer coefficients, respectively, cm/s
k_f = forward reaction rate constant of Eq. 9
k_r = backward reaction rate constant of Eq. 15
k_r', k_r'' = defined by Eq. 21 and Eq. 22, respectively
K_{eq} = equilibrium constant defined by Eq. 7
K_D', K_D'' = defined by Eq. 20 and Eq. 21, respectively
l = effective length of the module, cm
m_i = distribution coefficient of solute i between organic and aqueous phase, Eq. 6
N_F, N_S = total number of feed and strip side fibers, respectively
N_{Re} = Reynolds number, $4Q_F/\pi d_i^F \nu_w^F N_F$ for feed side, $4Q_S/\pi d_i^S \nu_w^S N_S$ for strip side
N_{Sc} = Schmidt number, ν_w^F/D_{iw}^F for feed side, ν_w^S/D_{iw}^S for strip side
N_{Sh} = Sherwood number, $k_i^F d_i^F/D_{iw}^F$ for feed side, $k_i^S d_i^S/D_{iw}^S$ for strip side
R_T = mass-transfer rate of Cu^{2+} per unit length of the module
$[\overline{RH}]$ = concentration of free oxime in the organic phase, mol/L
$[\overline{R_2Cu}]$ = concentration of copper-oxime complex in the organic phase, mol/L
q_1, q_2 = dimensionless volumetric flow rates, Eq. 36
Q_F = volumetric flow rate of the aqueous phase in the feed side, ml/min
Q^{ref} = reference volumetric flow rate of the aqueous phase, ml/min
Q_S = volumetric flow rate of the aqueous phase in the strip side, ml/min
S = dimensionless area defined by Eq. 36
t_{eff} = effective diffusion path from aqueous feed-organic interface to strip aqueous-organic interface, Eqs. 24 and 25
z = axial direction
Bracket [ ] = molar concentration, mol/L
overbar = organic phase

Greek letters

α = defined by Eq. 43
α_1, α_2, α_3 = defined by Eq. 45
β_j = constant defined by Eq. 35
δ_m = diffusion path length from feed fiber OD to strip fiber OD
δ_w = diffusion path length through the fiber wall
ϵ = porosity of membrane
ζ = dimensionless length, Eq. 36
η = viscosity of LIX 84 solution diluted in *n*-heptane, cp
ν_w = kinematic viscosity of aqueous phase, cm^2/s
ρ = specific gravity of LIX 84 solution diluted in *n*-heptane
τ = tortuosity of membrane pore

Superscripts

F = feed side
S = strip side

Subscripts

C = copper ion
F = feed side
Fb = bulk aqueous phase in the feed side
FI = feed-membrane interface at ID of the feed fiber
FO = feed-membrane interface at OD of the feed fiber
H = hydrogen ion
S = strip side
Sb = bulk aqueous phase in the strip side
SI = strip-membrane interface at ID of the strip fiber
SO = strip-membrane interface at OD of the feed fiber
t = total concentration of oxime in the organic phase, mol/L

Literature Cited

Basu, R., "Mass Transfer Enhancement in Phase Barrier Membrane Separators for Reactive Systems," PhD Diss., Stevens Institute of Technology, Hoboken, NJ (1990).
Basu, R., and K. K. Sirkar, "Hollow Fiber Contained Liquid Membrane Separation of Citric Acid," *AIChE J.*, **37**, 383 (1991).
Basu, R., and K. K. Sirkar, "Pharmaceutical Product Recovery using

a Hollow Fiber Contained Liquid Membrane: A Case Study," *J. Membrane Sci.*, **75**, 131 (1992).
Caban, R., and T. W. Chapman, "Losses of Mercury from Chlorine Plants: A Review of a Pollution Problem," *AIChE J.*, **18**(5), 904 (1972).
Danesi, P. R., "Separation of Metal Species by Supported Liquid Membranes," *Sep. Sci. Tech.*, **19**(11-12), 857 (1984, 1985).
Danesi, P. R., L. Reichley-Yinger, and P. G. Rickert, "Lifetime of Supported Liquid Membranes: The Influence of Interfacial Properties, Chemical Composition and Water Transport on the Long Term Stability of the Membranes," *J. Membrane Sci.*, **31**, 117 (1987).
Haan, A. B., P. V. Bartels, and J. Graauw, "Extraction of Metal Ions from Wastewater: Modeling of the Mass Transfer in a Supported Liquid-Membrane Process," *J. Membrane Sci.*, **45**, 281 (1989).
Hochhauser, A. M., and E. L. Cussler, "Concentrating Chromium with Liquid Surfactant Membranes," *AIChE Symp. Ser.*, **71**(152), 136 (1975).
Kiani, A., R. R. Bhave, and K. K. Sirkar, "Solvent Extraction with Immobilized Interfaces in a Microporous Hydrophobic Membrane," *J. Membrane Sci.*, **20**(2), 125, (1984).
Kim, B. M., "Membrane-based Solvent Extraction for Selective Removal and Recovery of Metals," *J. Membrane Sci.*, **21**, 5 (1984).
Komasawa, I., T. Otake, and T. Yamashita, "Mechanism and Kinetics of Copper Permeation through a Supported Liquid Membrane Containing a Hydroxyoxime as a Mobile Carrier," *Ind. Eng. Chem. Fund.*, **22**(1), 127 (1983).
Lee, K., D. F. Evans, and E. L. Cussler, "Selective Copper Recovery with Two Types of Liquid Membranes," *AIChE J.*, **24**, 860 (1978).
Majumdar, S., A. K. Guha, and K. K. Sirkar, "A New Liquid Membrane Technique for Gas Separation," *AIChE J.*, **34**, 1135 (1988).
Majumdar, S., A. K. Guha, Y. T. Lee, and K. K. Sirkar, "A Two-dimensional Analysis of Membrane Thickness in a Hollow-Fiber-Contained Liquid Membrane Permeator," *J. Membrane Sci.*, **43**, 259 (1989).
O'Hara, P. A., and M. P. Bohrer, "Supported Liquid Membranes for Copper Transport," *J. Membrane Sci.*, **44**, 273 (1989).
Pearson, D., "Supported Liquid Membranes for Metal Extraction from Dilute Solutions," *Ion Exchange Membranes*; Chapter 4, D. S. Flett, ed., Ellis Horwood Limited, Chichester (1983).
Prasad, R., and K. K. Sirkar, "Solvent Extraction with Microporous Hydrophilic and Composite Membranes," *AIChE J.*, **33**, 1057 (1987).
Prasad, R., and K. K. Sirkar, "Dispersion-Free Solvent Extraction with Microporous Hollow Fiber Modules," *AIChE J.*, **34**(2), 177 (1988).
Ritcey, G. M., and A. W. Ashbrook, *Solvent Extraction*, Part I; Elsevier, Amsterdam, 1984.
Sengupta, A., R. Basu, and K. K. Sirkar, "Separation of Solutes from Aqueous Solutions by Contained Liquid Membranes," *AIChE J.*, **34**, 1698 (1988a).
Sengupta, A., R. Basu, R. Prasad, and K. K. Sirkar, "Separation of Liquid Solutions by Contained Liquid Membranes," *Sep. Sci. Tech.*, **23**(12, 13), 1735 (1988b).
Sorenson, B. V., and R. W. Callahan, "Penicillin Separations with Contained Liquid Membranes," *Proc. ICOM*, **1**, 695 (1990).
Skelland, A. H. P., *Diffusional Mass Transfer*, Wiley, New York, p. 162 (1974).
Teramoto, M., and H. Tanimoto, "Mechanism of Copper Permeation through Hollow Fiber Liquid Membranes," *Sep. Sci. Tech.*, **18**, 871 (1983).
Teramoto, M., N. Tohno, N. Ohnishi, and H. Matsuyama, "Development of a Spiral-Type Flowing Liquid Membrane Module with High Stability and its Application to the Recovery of Chromium and Zinc," *Sep. Sci. Tech.*, **24**(12, 13), 981 (1989).
Thien, M. P., T. A. Hatton, and D. I. C. Wang, "Liquid Emulsion Membranes and Their Applications in Biochemical Separations," J. Asenjo and J. Hong, eds., *ACS Symp. Ser.*, 314, p. 67 (1986).
Weiss, S., V. Grigoriev, and P. Muhl, "The Liquid Membrane Process for the Separation of Mercury from Waste Water," *J. Membrane Sci.*, **12**, 119 (1982).
Williams, M. E., D. Bhattacharyya, R. J. Ray, and S. B. McCray, "Selected Applications," *Membrane Handbook*, Chapter 24, W. S. W. Ho and K. K. Sirkar, eds., Van Nostrand Reinhold, New York (1992).
Yi, J., and L. L. Tavlarides, "Chemically Active Liquid Membranes in Inorganic Supports for Metal Ion Separations," *AIChE J.*, **38**(12), 1957 (1992).
Yun, C. H., "Removal of Pollutants and Recovery of Toxic Heavy Metals from Wastewater using Microporous Hollow Fiber Modules," PhD Diss., Stevens Institute of Technology, Hoboken, NJ (1992).
Yun, C. H., A. K. Guha, and K. K. Sirkar, "Stability of the HFCLM Technique for Simultaneous Metal Removal and Concentration Processes," manuscript in preparation (1994).
Yun, C. H., R. Prasad, A. K. Guha, and K. K. Sirkar, "Hollow Fiber Solvent Extraction Removal of Toxic Heavy Metals from Aqueous Waste Stream," *Ind. Eng. Chem. Res.*, **32**(6), 1186 (1993).

Manuscript received June 9, 1993, and revision received Dec. 28, 1993.